Appendix 1 Characterization of Fluid Flow

The Reynolds number was calculated as follows:

$$Re = \frac{V * L}{\upsilon} = \frac{\frac{Q}{A} * L}{\left(\frac{\mu}{\rho}\right)} = \frac{Q\rho L}{\mu A} \quad (1)$$

where V is flow velocity (m/s), computed from the average fluid flow rate (m^3/s) and cross-sectional area (m) of the catheter (Q and A, respectively). L is characteristic length (m), and kinematic viscosity (m^2/s), υ, of the fluid is represented using dynamic viscosity (kg/m-s), μ, and density (kg/m^3), ρ. Using maximum fluid flow rate of 1120 cc/min (1.8667E-5 m^3/s) distributed equally across the two inlet catheters, density of water at 40 ℃ (992.2473 kg/m^3) (Ref. (1)), diameter of catheter (1.016 cm), dynamic viscosity of water at 40 ℃ (6.52E-4 kg/(m*s)) (Ref. (1)), and area of each catheter as $8.11x10^{-5}$ m^2, the maximum Reynolds number can be computed:

$$Re_{max} = \frac{\left(1.8667 * 10^{-5}\ \frac{m^3}{s}\right)\left(992.2473\ \frac{kg}{m^3}\right)(0.01016\ m)}{\left(6.52 * 10^{-4}\ \frac{kg}{m * s}\right)(8.11 * 10^{-5}\ m^2) * 2} \approx 1780. \quad (2)$$

In fully developed pipe flow, laminar flow occurs when Re < 2000.

Model of Fluid Flow

Momentum and continuity equations were solved using Reynolds (ensemble) averaging, in which scalar quantities and vector components in both equations (represented here generally as ϕ) are divided into mean ($\bar{\phi}$) and fluctuating (ϕ') components such that $\phi = \bar{\phi} + \phi'$. The Reynolds-averaged Navier-Stokes (RANS) equations for momentum and continuity equations are presented in Cartesian tensor form for i & $j \in \{1,2,3\}$ and dummy variable l for Einstein summation notation from Ref. (2):

$$\frac{\partial \rho}{\partial t} + \frac{\partial}{\partial x_i}(\rho \bar{u}_i) = 0 \quad (3)$$

https://dx.doi.org/10.21037/jgo-24-352

$$\frac{\partial}{\partial t}(\rho\bar{u}_i) + \frac{\partial}{\partial x_j}(\rho\bar{u}_i\bar{u}_j) = -\frac{\partial\bar{p}}{\partial x_i} + \frac{\partial}{\partial x_j}\left[\mu * \left(\frac{\partial\bar{u}_i}{\partial x_j} + \frac{\partial\bar{u}_j}{\partial x_i} - \frac{2}{3}\delta_{ij}\frac{\partial\bar{u}_l}{\partial x_l}\right)\right] + \frac{\partial}{\partial x_j}\left(-\rho\overline{u_i'u_j'}\right) \quad (4)$$

where ρ is fluid density, u is the velocity vector, p is static pressure, δ_{ij} is the Kronecker Delta, and $(-\rho\overline{u_i'u_j'})$ represents the Reynolds stresses. Specific dissipation rate (ω) and turbulence kinetic energy (k) were solved in SST from the baseline form, represented below from Ref. (2) in Equations 5 and 6 (with average bars dropped hereafter such that $\bar{\phi} = \phi$):

$$\frac{\partial}{\partial t}(\rho k) + \frac{\partial}{\partial x_i}(\rho k u_i) = \frac{\partial}{\partial x_j}\left[\Gamma_k\frac{\partial k}{\partial x_j}\right] + G_k - Y_k + S_k + G_b \quad (5)$$

$$\frac{\partial}{\partial t}(\rho\omega) + \frac{\partial}{\partial x_i}(\rho\omega u_i) = \frac{\partial}{\partial x_j}\left[\Gamma_\omega\frac{\partial\omega}{\partial x_j}\right] + G_\omega - Y_\omega + D_\omega + S_\omega + G_{\omega b} \quad (6)$$

where G_ω represents the generation of ω, G_k is the generation of k due to mean velocity gradients, D_ω represents the cross-diffusion term, and Γ_σ, S_σ, Y_σ, and $G_{\sigma b}$ represent effective diffusivity, source, dissipation in the turbulence, and buoyancy terms, respectively, of $\sigma \in \{k, \omega\}$. Lastly, in Ansys Fluent Reynolds stresses were modeled in the k-ω model using Boussinesq's hypothesis (Ref. (2)):

$$-\rho\overline{u_i'u_j'} = \mu_t\left(\frac{\partial u_i}{\partial x_j} + \frac{\partial u_j}{\partial x_i}\right) - \frac{2}{3}\left(\rho k + \mu_t\frac{\partial u_k}{\partial x_k}\right)\delta_{ij} \quad (7)$$

where μ_t is the turbulent viscosity. The SST form extends the baseline form by incorporating turbulent shear stress transportation into its definition of μ_t, thereby limiting eddy-viscosity formation (Ref. (2)):

$$\mu_t = \frac{\rho k}{\omega} * \frac{1}{\max\left[\frac{1}{\alpha^*}, \frac{S * F_2}{\alpha_1 * \omega}\right]} \quad (8)$$

$$F_2 = \tanh(\Phi_2^2) \quad (9)$$

$$\Phi_2 = \max\left[\frac{2\sqrt{k}}{0.09\omega y}, \frac{500\mu}{\rho y^2\omega}\right] \quad (10)$$

$$\alpha^* = \alpha_\infty^* \cdot \left(\frac{\alpha_0^* + Re_t/R_k}{1 + Re_t/R_k}\right) \quad (11)$$

https://dx.doi.org/10.21037/jgo-24-352

$$Re_t = \frac{\rho k}{\mu \omega} \tag{12}$$

$$\alpha_0^* = \frac{\beta_i}{3} \tag{13}$$

where α^* is dampening coefficient for turbulent viscosity, $\alpha_1 = 0.71$, $\alpha_\infty^* = 1$, $R_k = 6$, $\beta_i = 0.072$, S is strain rate magnitude, and y is distance to adjacent surface. Other parameter values used by Ansys Fluent for SST k-ω modelling are as in Ref. (2).

Model of Heat Transport

Energy of fluids was modeled in Ansys Fluent using the equations from Ref. (2) for each fluid species j:

$$\frac{\partial}{\partial t}\left(\rho\left(e + \frac{v^2}{2}\right)\right) + \nabla \cdot \left(\rho v \left(h + \frac{v^2}{2}\right)\right) = \nabla \cdot \left(k_{eff}\nabla T - \sum_j h_j \vec{J}_j + \bar{\bar{\tau}}_{eff} \cdot \vec{v}\right) + S_h \tag{14}$$

where the four terms on the right-hand side represent, from left to right, energy transfer due to conduction, species diffusion, viscous dissipation, and volumetric heat sources. Here, viscous dissipation and volumetric heat sources were not modeled and are assumed negligible. Thus, Equation 14 was simplified in this study to:

$$\frac{\partial}{\partial t}\left(\rho\left(e + \frac{v^2}{2}\right)\right) + \nabla \cdot \left(\rho v \left(h + \frac{v^2}{2}\right)\right) = \nabla \cdot \left(k_{eff}\nabla T - \sum_j h_j \vec{J}_j\right) \tag{15}$$

where k_{eff} is the effective conductivity obtained as the sum of the thermal conductivity k and turbulent thermal conductivity k_t, $\vec{J}_j$ is the diffusion flux of species j, and ρ, v, e, and T are the density, velocity, internal energy, and temperature of the fluid, respectively. For a simulation of a single fluid species, enthalpy, h, is computed as

$$h = h_j = \int_{T_{ref}}^{T} c_{p,j}\, dT + \frac{p}{\rho} \tag{16}$$

where $c_{p,j}$ is the isobaric specific heat for j, p is the gauge pressure, T is fluid temperature, and T_{ref} is 298.15 K for Ansys' pressure-based solver. The internal energy e is defined as

https://dx.doi.org/10.21037/jgo-24-352

$$e = h - \frac{p_{op} + p}{\rho} \tag{17}$$

where p_{op} is the operating pressure.

For solids, the energy transport for a solid with isotropic heat conductivity was simulated as given for Ansys Fluent in Ref. (2):

$$\frac{\partial}{\partial t}(\rho h) + \nabla \cdot (\vec{v}\rho h) = \nabla \cdot (k\nabla T) + S_h \tag{18}$$

where ρ, k, T, and S_h are the solid's density, conductivity, temperature, and volumetric heat source term, respectively, for the solid and are defined analogously to their liquid counterparts. The sensible enthalpy of the solid, h, is computed as $h = \int_{T_{ref}}^{T} c_p \, dT$. Because motion of organs and the abdominal cavity is not considered in this model, the velocity field $\vec{v} = 0$. Since this study did not use volumetric heat sources, $S_h = 0$. Thus, Equation 18 simplifies in this study to:

$$\frac{\partial}{\partial t}(\rho h) = \nabla \cdot (k\nabla T) \tag{19}$$

Grid and Time Step Independence

Grid independence was ensured through mesh sensitivity analysis of outlet temperature (**Figure** S1**A**) and probes (**Figure** S1**B**) across three mesh resolutions: low (158859 nodes and 803073 elements), medium (212444 nodes and 1069090 elements), and high (786837 nodes and 4081208 elements). Across all tests, inlet flow rate was held constant at 1100 cc/min. Differences between meshes remained within 0.2 ℃ of outlet temperature. For probes, temperature changes between meshes were <0.3 ℃. Thus, the medium resolution mesh was chosen.

Time step independence was determined through time step sensitivity analysis for both the outlet temperature (**Figure S1C)** and the temperature for each probe location at 5400s (**Figure S1D**). Time step sizes analyzed were 0.0625s, 0.25s, and 1s. Outlet temperatures and probe location temperatures were within 1E-2 ℃ regardless of time step size selected. Therefore, 0.25s was chosen for the analysis.

 https://dx.doi.org/10.21037/jgo-24-352

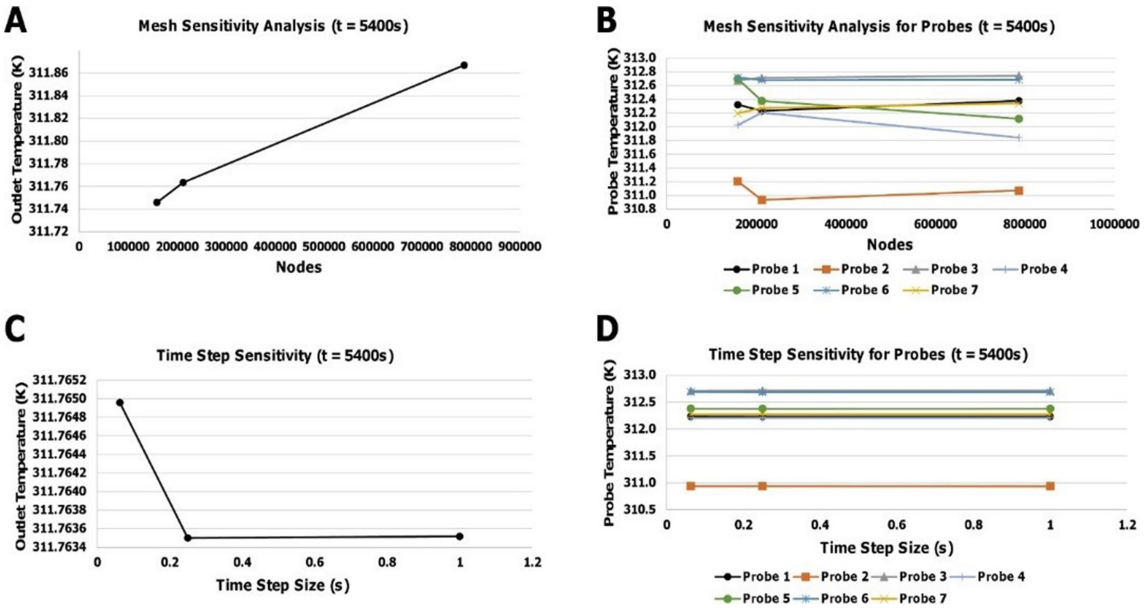

Figure S1 Grid and time step sensitivity analysis. (A) Mesh analysis of outlet temperature and (B) probe temperatures with low, medium, and high resolution. (C) Time step analysis of outlet temperature and (D) probe temperatures at time step sizes of 0.0625 s, 0.25 s, and 1 s. Probe locations; 1: between small and large bowels; 2: inferior to small bowel mesentery; 3: next to duodenum; 4: superior to liver; 5: superior to fundus; 6; posterior to stomach; 7: posterior to liver.

References

1. Kestin J, Sokolov M, Wakeham WA. Viscosity of liquid water in the range –8 °C to 150 °C. J Phys Chem Ref Data 1978;7:941-8.
2. Ansys Fluent Theory Guide: Ansys, Inc.
3. Hasgall PA, Di Gennaro F, Baumgartner C, et al. IT'IS database for thermal and electromagnetic parameters of biological tissues, 2018. Available online: www.itis.ethz.ch/database
4. Blinzler BJ, Khalili P, Ahlström J. Integrated Computational Material Design for PMC Manufacturing with Trapped Rubber. Materials (Basel) 2020;13:3825.

https://dx.doi.org/10.21037/jgo-24-352

Table S1 Material properties used for simulations [data from (3,4)]

Component	Density (kg/m^3)	Heat capacity (J/(kg·℃))	Thermal conductivity (W/(m·℃))
Stomach	1,088	3,690	0.53
Liver	1,079	3,540	0.52
Transverse Colon	1,088	3,655	0.54
Small Bowel	1,030	3,595	0.49
Silicone Rubber	1,400	1,175	0.60

Table S2 Dimensions of abdominal cavity and organs simulated using SOLIDWORKS

Component	Height (cm)	Depth (cm)	Width (cm)
Cavity	58.7	24.7	39.8
Transverse Colon	7.0	5.1 (diameter)	39.4
Stomach	11.2	6.9	18.5
Esophagus	10.6	7.0	2.8 (diameter)
Small Bowel	22.9	15.2	20.3 (diameter)
Liver	19.9	19.6	35.6 (apex to apex)

https://dx.doi.org/10.21037/jgo-24-352